



# Nanofiller concentration-dependent appreciably tailorable and multifunctional properties of (PVP/PVA)/SnO<sub>2</sub> nanocomposites for advanced flexible device technologies

R. J. Sengwa<sup>1,\*</sup>  and Priyanka Dhatarwal<sup>1</sup>

<sup>1</sup> Dielectric Research Laboratory, Department of Physics, Jai Narain Vyas University, Jodhpur 342 005, India

**Received:** 5 October 2020

**Accepted:** 23 February 2021

**Published online:**  
13 March 2021

© The Author(s), under exclusive licence to Springer Science+Business Media, LLC, part of Springer Nature 2021

## ABSTRACT

Polymer nanocomposites (PNCs) are currently in high industrial demand for the development of a variety of technologically advanced flexible-type milli- to micro-sizes electronic components/devices. In the advances of PNC materials, herein, we have prepared the hybrid nanocomposite films taking tin oxide (SnO<sub>2</sub>) nanoparticles as filler and biodegradable poly(vinyl pyrrolidone)/poly(vinyl alcohol) (PVP/PVA) blend as host matrix. Analysis of X-ray diffraction (XRD) patterns, Fourier transform infra-red (FTIR) spectra, and the scanning electron microscope (SEM) images have shown the successful formation of these (PVP/PVA)/SnO<sub>2</sub> nanocomposites. The percent degree of crystallinity of the nanocomposites and the diffraction peak intensities of the SnO<sub>2</sub> filler in these hybrids were found to increase linearly when the filler concentration was enhanced from 1 to 5 wt%. Differential scanning calorimetry (DSC) thermograms confirmed that the SnO<sub>2</sub> nanoparticles dispersion in the PVP/PVA matrix has led to an appreciable increase in the thermal properties of these composite materials. Ultraviolet–visible (UV–Vis) range spectroscopic measurements revealed that these PNC materials have the ability of UV radiation absorption in a controllable manner. The direct and indirect energy band gaps of these PNCs had systematically reduced up to that of the SnO<sub>2</sub> band gap confirming them as band gap tunable optical materials. The results of dielectric relaxation spectroscopy (DRS) performed over the 20 Hz to 1 MHz frequency range revealed that the dielectric permittivity and also the electrical conductivity could be enhanced appreciably by increasing amounts of SnO<sub>2</sub> nanoparticles in the PVP/PVA blend host matrix. The SnO<sub>2</sub> nanofiller concentration-dependent effectively tailorable structural, thermal, optical, and dielectric parameters credit the multifunctionality of these biodegradable PNCs. Therefore, it is concluded that these flexible hybrid films could be useful in the realization of desirable design and workability of the next-generation variety of

Address correspondence to E-mail: rjsengwa@rediffmail.com; rjs.ph@jnvu.edu.in

advanced optoelectronic, organoelectronic, and microelectronic components/devices.

## 1 Introduction

Amorphous poly(vinyl pyrrolidone) (PVP) and semicrystalline poly(vinyl alcohol) (PVA) are non-toxic, biodegradable, water-soluble, easily processable, and transparent film-forming polar polymers of modest thermal and mechanical properties. These properties have accredited both PVP and PVA as potential candidates for a wide range of technological as well as biomedical applications [1, 2]. The pristine PVP and PVA films have low values of dielectric permittivity and also poor electrical conduction behavior over a broad frequency range [3, 4] which confirm their suitability as low-dielectric biodegradable and transparent materials. The controllable useful properties of the solid-state complexes/composites of these polymers with different dopants/fillers have established them highly suitable in designing several lightweight and flexible-type biodegradable microelectronic, organoelectronic, and optoelectronic devices [3–12]. The carbonyl (C=O) and hydroxyl (–OH) groups of the PVP and PVA chain repeat units, respectively, have formed highly effective interactions with the inorganic and organic nanofillers which have resulted in promising properties composites [1–12].

The hydrogen bonding ability of the C=O and –OH groups of the PVP and PVA together form a miscible blend of several improved properties [13, 14]. Hence, the PVP/PVA blend is greatly preferred in the preparation of a variety of composite materials with the integration of suitable properties dopants/nanofillers [15–26]. The nanofiller-loaded polymer matrix-based PNCs are relatively low-cost flexible materials having several tailorable and improved properties [10–12, 17, 18, 27, 28]. Many studies have concluded that the flexible nature, durability, chemical resistance, lightweight, thermomechanical stability, etc. of the PNC materials are primarily governed by the appropriately selected host polymer matrix. But these properties can also be modified in a tailorable manner over a broad range by incorporating nanomaterials of effective properties during the development of the technologically important PNC materials.

With regard to the advances in flexible-type optoelectronic, organoelectronic, and sensing devices made of PNC materials, the SnO<sub>2</sub> nanoparticles (NPs) dispersed PNC films have received much attention in the past few years [3, 8, 21, 24, 27–33]. The SnO<sub>2</sub> nanomaterial is a high crystallinity compound semiconductor that has a wide energy band gap (~ 3.6 eV) and extremely appealing technological importance [34–36]. Until now, the literature survey has manifested that the systematic investigation on the structural properties as well as the thermal, optical, and dielectric behavior of the PVP/PVA blend dispersed with a low amount of SnO<sub>2</sub> NPs are less attempted [21, 24]. In the last decade, the development of a variety of PNCs and their systematic characterization for exploring their various technologically useful promising properties, especially the dielectric dispersion and electrical conduction behavior, have remained a thrust research area of many researchers [3, 9, 10, 15–20, 25, 32, 37–42]. The main focus on the dielectric characterization of PNCs is highly advantageous because the dielectric and electrical parameters are decisive properties for their uses as flexible- and stretchable-type polymer nanodielectric (PND) in the development of high-performance multifunctional devices [37–39, 41, 43–45]. If a particular device can work for different applications e.g., as a sensor, an absorber, UV shielder, band gap tuner, band blocker/filters, etc., depending on the wavelength of illuminating photons, then such device categorizes as a multifunctional optical device [9, 38]. Similarly, if a device can be used as a current regulator, adjustable resistor, and energy generator/convertor, then it is called a multifunctional electrical device [18, 41].

Herein, we have successfully developed the (PVP/PVA)/SnO<sub>2</sub> nanocomposite films by solution casting method. The effect of SnO<sub>2</sub> nanofiller contents on the optical, dielectric, and thermal properties of these films has been characterized by engaging advanced UV–Vis and dielectric spectroscopy, and differential scanning calorimetry. This study mainly focuses on examining the SnO<sub>2</sub> concentration-dependent tailorable thermal, optical, and dielectric parameters along with the structural properties of the (PVP/

PVA)/SnO<sub>2</sub> films in relation to confirm their multifunctional device applications.

## 2 Experimental

### 2.1 Materials and PNCs preparation

PVP fine powder ( $M_w = 6 \times 10^5 \text{ g mol}^{-1}$ ) of S.D. Fine-Chem Ltd., Mumbai, India, PVA granular powder ( $M_w = 77 \times 10^3 \text{ g mol}^{-1}$ ) of Loba Chemie Pvt. Ltd., Mumbai, India, and SnO<sub>2</sub> nanopowder of particle sizes lower than 100 nm which is a product of Sigma-Aldrich Co., USA were taken for the preparation of (PVP/PVA)/SnO<sub>2</sub> films. These films were prepared by homogeneous mixing in the deionized water followed by the solution casting method. In the beginning, transparent aqueous polymeric solutions of equal amounts (0.50 g each) of PVP and PVA were prepared in deionized water (20 ml) in separate conical flasks. The PVA was dissolved at about 90 °C with continuous magnetic bar stirring using microprocessor-fitted temperature-controlled magnetic stirrer, whereas the PVP completely dissolved at 30 °C just above the ambient temperature. Then these polymeric solutions were mixed to get a PVP/PVA blend solution of 50/50 wt% compositional ratio. The suspensions of SnO<sub>2</sub> NPs amounts for their 1 wt%, 3 wt%, and 5 wt% concentration in comparison to that of the total amount used for PVP/PVA blend were separately made in deionized water with sonication and then strong magnetic bar stirring. Thereafter, these amounts of NPs suspensions were mixed with the previously prepared respective PVP/PVA blend solutions which resulted in (PVP/PVA)/SnO<sub>2</sub> suspensions of varying SnO<sub>2</sub> concentrations. These solutions were again sonicated till the homogeneously viscous hybrid polymeric solutions were formed. Finally, they were transferred into polypropylene petri dishes and kept to dry, which formed stable and flexible-type (PVP/PVA)/SnO<sub>2</sub> films. These PNC films were vacuum-dried overnight at 60 °C and then their different characterizations were performed.

### 2.2 Measurements

XRD patterns of the (PVP/PVA)/SnO<sub>2</sub> films and also pristine SnO<sub>2</sub> nanopowder were measured at room

temperature using X'pert Pro MPD of PANalytical, The Netherlands. These patterns were recorded in the reflection mode operation for Cu-K<sub>α</sub> radiation ( $\lambda = 1.5406 \text{ \AA}$ ) with the scanning speed of 3 °/min. The microscale images of these films upper surfaces were constructed with Zeiss EVO MA15 scanning electron microscope (SEM) operated at 20 kV beam voltage. FTIR spectra were captured for these PNC films under ATR mode using the Cary 630 FTIR spectrometer of Agilent Technologies. Thermograms of the PNC samples were recorded with DSC of TA Instruments under the atmosphere of dried nitrogen flow with a 10 °C/min heating rate.

The UV–Vis absorption spectra of the (PVP/PVA)/SnO<sub>2</sub> films in the wavelength range 200–800 nm were recorded at ambient temperature with a Cary 60 UV–Vis spectrophotometer of Agilent Technologies. The electrical measurements were performed under an alternating current (AC) electric field in the 20 Hz to 1 MHz frequency range and of 1-V amplitude. The film was mounted for measurements between 38 mm diameter circular plate electrodes of the 16451B solid dielectric test fixture compatible with 4284A precision LCR meter (both of Agilent Technologies). The test fixture was kept in a microprocessor thermostated oven for the electrical measurements of the films at a controlled temperature.

## 3 Results and discussion

### 3.1 Analysis of XRD patterns

The XRD patterns in the  $2\theta$  range 10°–70° of the (PVP/PVA)/ $x$  wt% SnO<sub>2</sub> films having  $x$  values 0 wt%, 1 wt%, 3 wt%, and 5 wt% are depicted in Fig. 1. The prominent diffraction peak that appeared at  $2\theta = 19.56^\circ$  in the XRD pattern of PVP/PVA blend film without nanofiller (i.e.,  $x = 0$  wt%) is attributed to the PVA crystallites [42]. It is because of the fact that the PVP is amorphous material which showed its diffused halos centered at  $2\theta \simeq 12^\circ$  and  $2\theta \simeq 22.5^\circ$  [3, 42]. The SnO<sub>2</sub> nanopowder diffraction peaks positions labeled with indices on the XRD trace given in Fig. 1 and their relative intensities confirm the tetragonal rutile structure of SnO<sub>2</sub> crystallites demonstrated in detail elsewhere [31, 34–36]. All these PNC films exhibited the characteristic peak of semicrystalline PVA and also the different peaks of

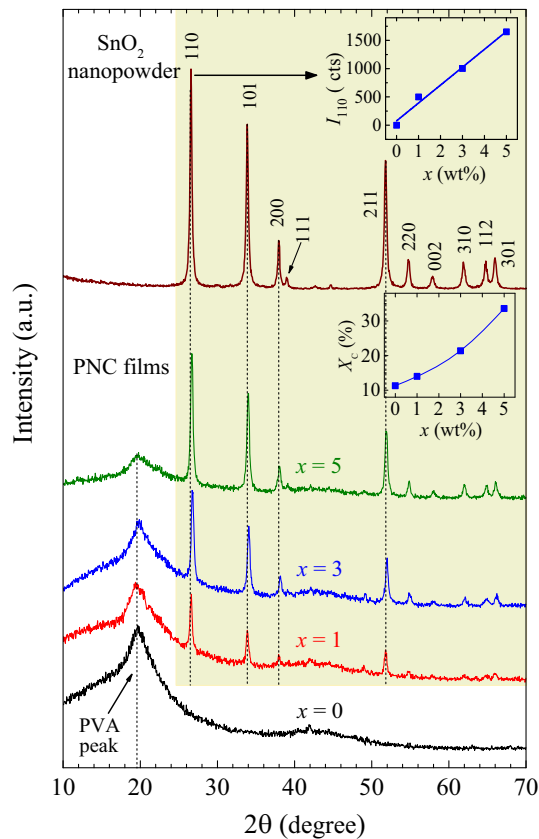


**Fig. 1** The XRD patterns of (PVP/PVA)/ $x$  wt% SnO<sub>2</sub> films and the SnO<sub>2</sub> nanopowder. The insets display the SnO<sub>2</sub> peak intensity  $I_{110}$  and percent crystallinity  $X_c$  versus  $x$  (wt%) plots

highly crystalline SnO<sub>2</sub> NPs confirming the semicrystalline nature of these hybrid composites.

It is observed from the comparative shape of the XRD patterns of these PNC films (see Fig. 1) that the loaded SnO<sub>2</sub> NPs (1–5 wt%) in the PVP/PVA blend matrix have altered either the intensity or the position of the PVA diffraction peak. However, all the characteristic peaks of SnO<sub>2</sub> appeared at the same positions with increasing intensities when there was a rise in the loaded nanofiller amount in the host matrix. The XRD traces of these PNC films revealed their several structural characteristics: (i) the changes in the PVA peak intensity attribute to some kind of polymer-NPs interactions due to which the crystallites of PVA got modified and hence the percent crystallinity of the PVP/PVA matrix have altered, (ii) the increase in intensities of the SnO<sub>2</sub> peaks corroborated to the existence of more number of loaded NPs in the polymer structures with the increase of nanofiller contents, (iii) there was no variation noted in the positions of SnO<sub>2</sub> peaks which revealed that the NPs

of the filler have retained their crystal structure in these composite films, and (iv) a linear increase of the SnO<sub>2</sub> peak intensities with the increase of nanofiller concentration (e.g.,  $I_{110}$  versus  $x$  (wt%)) in the plot shown in the inset of Fig. 1 confirmed the homogeneous existence of the dispersed NPs in the structure of host matrix. This finding evidences the successful formation of these hybrid nanocomposites prepared by the solution casting method. This fact was considered and demonstrated for good hybrid formation in a number of PNC materials prepared with crystallite nanofillers [3, 33, 38, 39].

The percent degree of crystallinity  $X_c$  (%) of these semicrystalline (PVP/PVA)/SnO<sub>2</sub> materials was determined considering the total area of the diffraction peaks  $A_c$  and hump area  $A_a$ -based crystallinity relation  $X_c$  (%) =  $(A_c/(A_c + A_a)) \times 100$  as given in the literature [32]. The computation procedure of both these areas from the XRD pattern is explained in detail elsewhere [40]. The observed  $X_c$  values for these PNCs are plotted against nanofiller concentration  $x$  (wt%) in the lower inset of Fig. 1. It is clear from this plot that the crystalline amount of these hybrid composites enhanced with the increase of SnO<sub>2</sub> concentration which was expected due to the fact that the crystallinity of the SnO<sub>2</sub> nanofiller is relatively very high (~ 84%) [41].

### 3.2 FTIR spectra and polymer-NPs interactions

Figure 2 depicts the FTIR spectra of (PVP/PVA)/SnO<sub>2</sub> films in the wavenumber range of 400–4000 cm<sup>-1</sup>. The 1800–2700 cm<sup>-1</sup> range has been omitted from these FTIR spectra because there was no vibrational band in this range, and clarity of other range bands also increased by this presentation. The vibrational bands of the PVP/PVA structures are labeled with their wavenumbers in this figure. Vertical dashed lines are drawn as a reference for the comparative analysis of these PNC films bands (position and intensity) with that of the host PVP/PVA blend matrix ( $x = 0$  wt%). According to the literature, it was noted that the PVP/PVA blend film ( $x = 0$  wt%) exhibited most of the characteristic bands of the PVP structure and that of the PVA structure with some alterations in their positions confirming that these macromolecules form C=O···H–O hydrogen-bonded heterogeneous networks [16, 20, 26, 39]. In brief, these bands are summarized here for the benefit

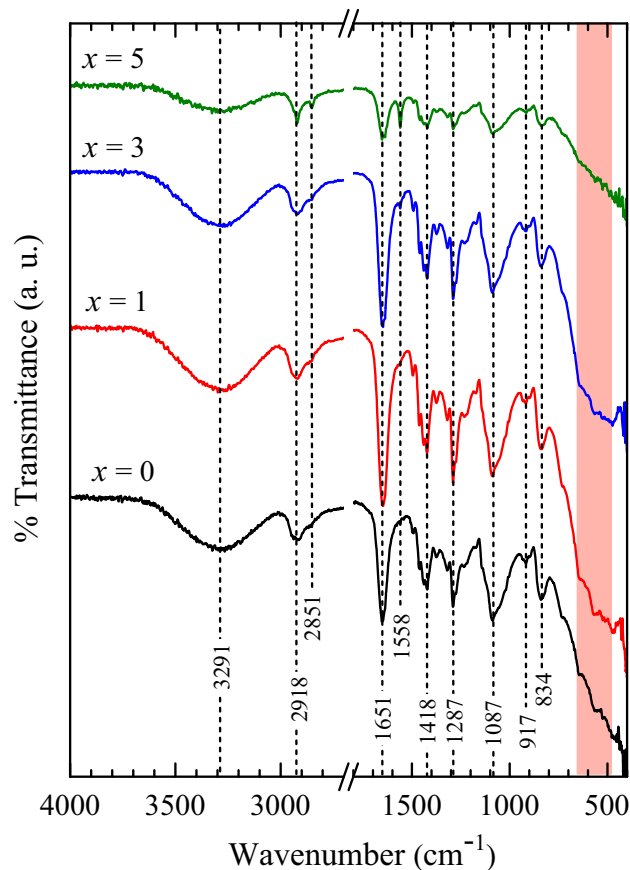


**Fig. 2** FTIR spectra of (PVP/PVA)/ $x$  wt% SnO<sub>2</sub> films. The wavenumbers corresponding to major vibrational bands of the PVP/PVA host matrix ( $x = 0$  wt%) are labeled with vertical dashed lines that are a guide to the eye. The highlighted part by light peach color belongs to the SnO<sub>2</sub> vibrational bands

of the readers. All these PNCs have a broader band centered at about 3291 cm<sup>-1</sup> belonging to the -OH group stretching vibration which is a constituent of the PVA chain repeat units. A weak-intensity band corresponding to the C-H asymmetric stretching mode of both the PVP and PVA was noted at 2918 cm<sup>-1</sup>, whereas the C-H symmetric stretching band has appeared at 2851 cm<sup>-1</sup> which became gradually intense with the increase of SnO<sub>2</sub> amount in the PVP/PVA matrix. Furthermore, a highly intense band corresponding to the stretching vibrational mode of the C=O groups present in the PVP structure has evolved at 1651 cm<sup>-1</sup> which is expected according to the literature [16, 39]. The bands noted at 1418 cm<sup>-1</sup> and 1287 cm<sup>-1</sup> can be assigned to the CH<sub>2</sub> wagging and asymmetric CH<sub>2</sub> twisting modes, respectively. The bands of C-O and C-C stretching vibrational modes were noted at 1087 cm<sup>-1</sup> and

834 cm<sup>-1</sup>, respectively, which belong to both the PVA and PVP molecules in the polymer blend [26].

A closer look at the FTIR spectra of (PVP/PVA)/SnO<sub>2</sub> composite materials revealed that there were some changes in intensities and shapes of all the above-mentioned vibrational bands of the PVP/PVA blend in the composites. Further, there is the appearance of an additional band at 1558 cm<sup>-1</sup> which can be noted stronger in the FTIR spectrum of 5 wt% filler concentration PNC film. Further, a little shift in the position of a few bands was also observed. The Sn-O and O-Sn-O stretching vibrational modes of SnO<sub>2</sub> NPs are exhibited in the wavelength span of 540–660 cm<sup>-1</sup>. The highlighted portion by light peach color in Fig. 2 has some signature of the SnO<sub>2</sub> NPs vibrational bands in these composites. All these observations evidence that the SnO<sub>2</sub> NPs with their geometrical confinement in the polymer matrix have formed the electrostatic interactions and probably some charge transfer complexations (CTCs) with the structures of PVP/PVA blend in these hybrid composites.

### 3.3 SEM images and morphology

The SEM images of (PVP/PVA)/SnO<sub>2</sub> films are collected in Fig. 3 and the same were analyzed for exploring the morphological changes in the top surface (i.e., the solvent evaporated surface) of these films. It is clear from Fig. 3a that the surface of the PVP/PVA blend film was highly homogeneous and smooth confirming that the PVP and PVA molecules exhibited high compatibility and formed a miscible blend [17, 24, 26, 39]. On the dispersion of SnO<sub>2</sub> NPs, some roughness on the surface of these hybrid composite films was noted which evidence some interactions between the polymer and NPs, and this finding is in agreement with their XRD and FTIR results. Further, it appears from the inspection of these SEMs that there was a uniform distribution of the loaded SnO<sub>2</sub> NPs in the blended PVP/PVA matrix. The results of these SEMs also evidence the successful creation of these nanocomposites and support the outcomes of their XRD analysis in this regard demonstrated in the previous section. Further, the micrographs of these composite films are found in good agreement with the earlier reported findings [24].

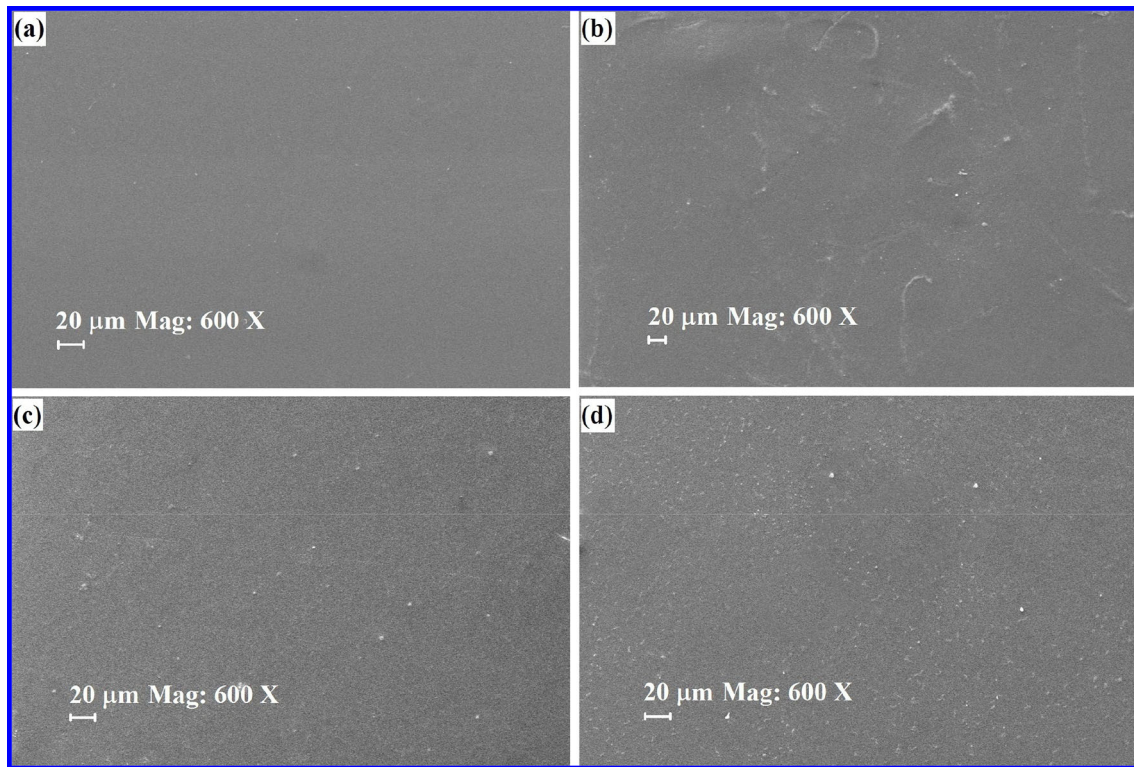


**Fig. 3** SEM images of (PVP/PVA)/ $x$  wt% SnO<sub>2</sub> films for **a**  $x = 0$ , **b**  $x = 1$ , **c**  $x = 3$ , and **(d)**  $x = 5$

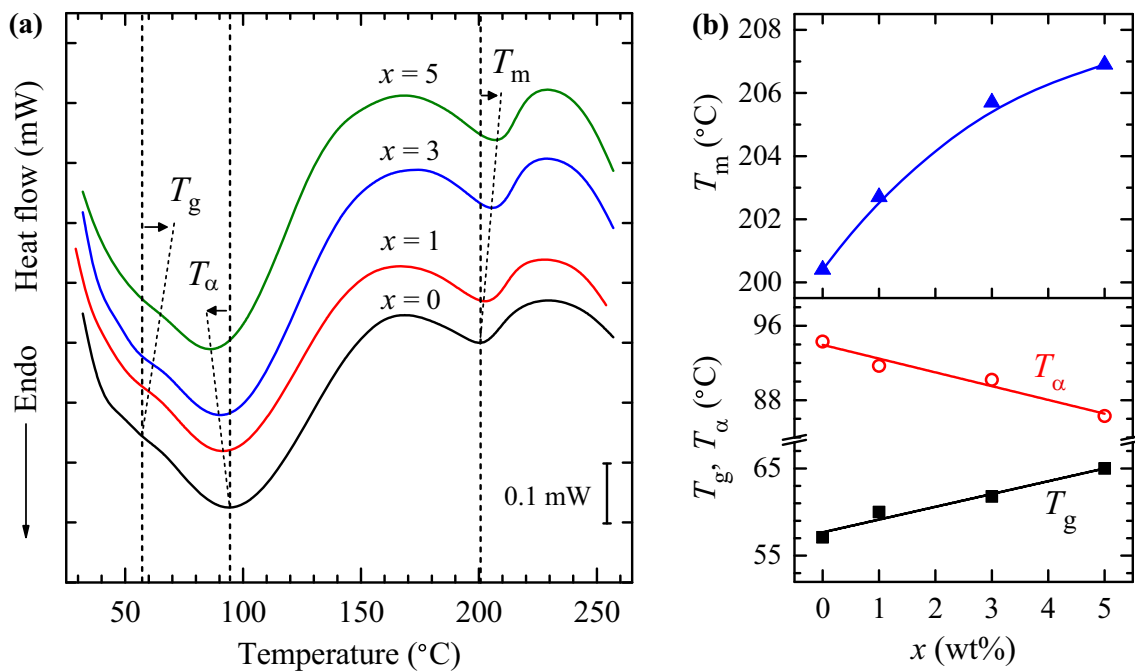
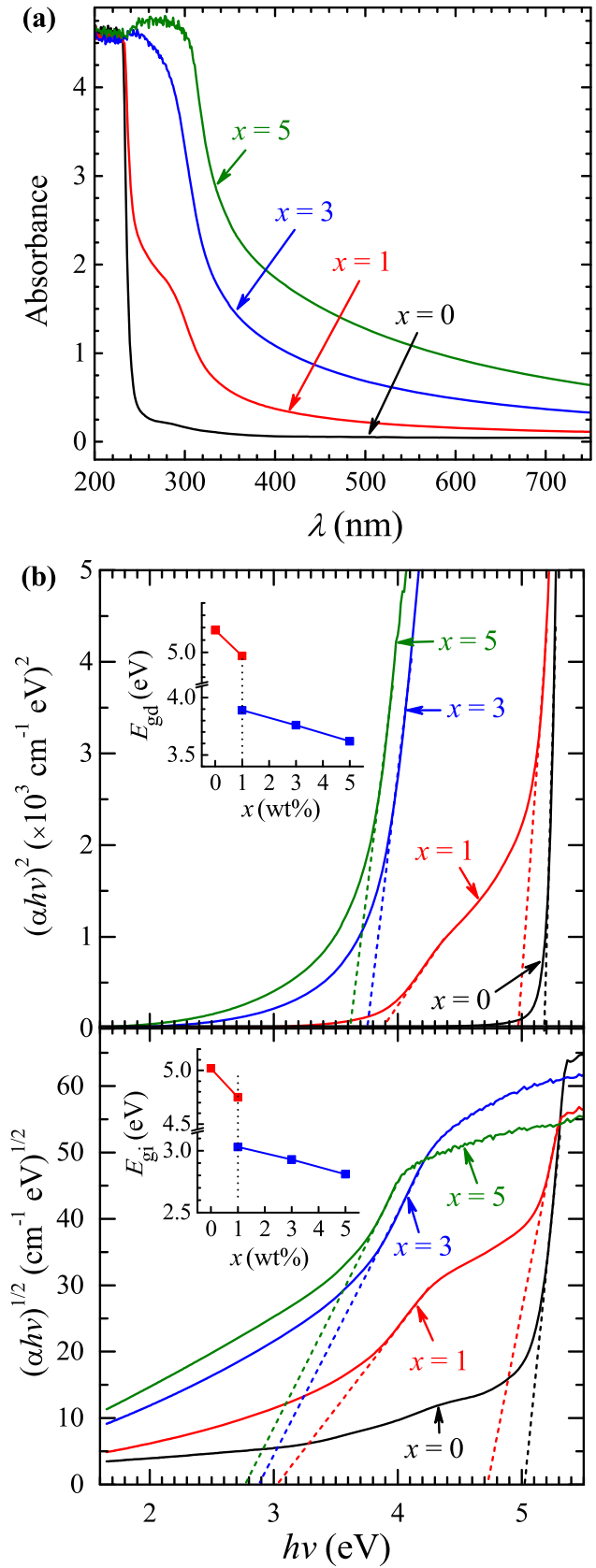


**Fig. 4** **a** DSC thermograms of (PVP/PVA)/ $x$  wt% SnO<sub>2</sub> films for  $x = 0, 1, 3,$  and  $5$  and **b** the plots of  $T_g$ ,  $T_\alpha$ , and  $T_m$  versus  $x$  (wt%) of nanofiller for these PNC films

### 3.4 DSC thermograms and thermal parameters

Figure 4a shows the thermograms of (PVP/PVA)/SnO<sub>2</sub> films in the temperature range from 30 to 257 °C. In this figure, the DSC curves of all the PNC films are set in a vertical shift with increasing SnO<sub>2</sub> concentration in the films. The heat flow scale is also marked for a better comparison of the thermal processes noted in these PNC films. The glass transition temperature  $T_g$ , the  $\alpha$ -relaxation temperature of micro-Brownian chain motion  $T_\alpha$  and the melting phase transition temperature  $T_m$  of these hybrid PNC films are marked with slanted dashed lines in the figure. The  $T_g$ ,  $T_\alpha$  and  $T_m$  values of the PVP/PVA blend film were found to be 57.1 °C, 94.3 °C, and 200.4 °C, respectively, which are in agreement with the earlier reported results [17, 24].

A single  $T_g$  value observed for the PVP/PVA blend attributes to good miscibility of the blended polymers at their 50/50 wt% compositional ratio especially in their amorphous regions as explained in the literature [17]. Figure 4b confirms that the  $T_g$  values enhanced linearly from 57.1 to 65 °C with the rise of SnO<sub>2</sub> amounts from 0 to 5 wt% in these hybrid composites. This finding indicates that the dispersed SnO<sub>2</sub> NPs act as hardner for the surrounding heterogeneous structures of the PVP/PVA blend. In contrast to  $T_g$  values, the  $T_\alpha$  values gradually decreased from 94.3 to 86.3 °C with the increase of SnO<sub>2</sub> concentration revealing that the segmental mobility of the H-bonded polymer blend structures had been enhanced. The observed  $T_\alpha$  values also suggest that there may be a decrease in either the strength or density of polymer–polymer H-bond heterogeneous interactions in the polymeric domains which is due to the formation of polymer-NPs interactions in the NPs surrounded polymeric domains. This may be the reason due to which the micro-Brownian motion was facilitated in the blended PVP/PVA structures. The increase of  $T_m$  values from 200.4 to 206.9 °C with the rise in the loading of SnO<sub>2</sub> NPs up to 5 wt% in the PVP/PVA blend (see the upper layer of Fig. 4b) evidenced the increased thermal stability of the composite films.



◀ **Fig. 5** **a** UV–vis absorbance spectra and **b** plots of  $(\alpha hv)^2$  versus  $hv$  and  $(\alpha hv)^{1/2}$  versus  $hv$  of (PVP/PVA)/ $x$  wt% SnO<sub>2</sub> films for  $x = 0, 1, 3, \text{ and } 5$ . Insets of **b** show the plots of direct energy band gap ( $E_{gd}$ ) and indirect energy band gap ( $E_{gi}$ ) versus  $x$  (wt%) concentration of nanofiller

### 3.5 UV–Vis absorbance spectra and energy band gap

The UV–Vis absorbance versus wavelength  $\lambda$  plots for the (PVP/PVA)/SnO<sub>2</sub> films are depicted in Fig. 5a. A sharp absorption edge was noted around 240 nm for the PVP/PVA blend film without nanofiller ( $x = 0$  wt%), whereas the absorbance was insignificant for the photons of higher wavelengths ( $\lambda > 240$  nm). One can see from these UV–Vis spectra that the absorption edge progressively moved towards a higher wavelength when the SnO<sub>2</sub> content was increased in these PNC films. The wavelength-dependent appreciable enhancement in lower wavelengths UV absorbance with increasing the SnO<sub>2</sub> concentration infers the suitability of (PVP/PVA)/SnO<sub>2</sub> films as wavelength tunable UV shielders [38, 41]. Further, the 1 wt% of SnO<sub>2</sub>-loaded PNC film exhibited double-absorbance edges which are around 320 nm and 250 nm, whereas the 3 wt% and 5 wt% concentrations composite films displayed single absorbance edge relatively at higher UV wavelength. Further, these absorbance bands of the nanocomposites shifted towards the high wavelength side with increasing nanofiller concentration from 3 to 5 wt%. These spectra clearly evidenced that the 1 wt% of SnO<sub>2</sub>-loaded PNC film have electronic transitions of the PVP/PVA blend structures as well as of the SnO<sub>2</sub> material, whereas the 3 wt% and 5 wt% of SnO<sub>2</sub>-loaded PNC films exhibited the transitions of SnO<sub>2</sub> structures only. This is a highly appealing characteristic of the (PVP/PVA)/SnO<sub>2</sub> films for their suitability in photoelectronic and sensor applications [25, 26, 30, 38].

To analyze the direct and indirect band gap energies of these (PVP/PVA)/SnO<sub>2</sub> materials, firstly the wavelength-dependent absorption coefficient was determined and then the respective Tauc's plots [46] i.e.,  $(\alpha hv)^2$  versus photon energy  $hv$  and  $(\alpha hv)^{1/2}$  versus  $hv$  were plotted in Fig. 5b. From these plots, direct energy band gap  $E_{gd}$  and the indirect energy band gap  $E_{gi}$  values of the PNC films were determined by extrapolating the tangent drawn on the linear

segments of the plots to the zero value on the abscissa (as marked by slanted dashed lines in the figure). The observed  $E_{gd}$  and  $E_{gi}$  values are plotted against the SnO<sub>2</sub> concentration  $x$  (wt%) in the insets of Fig. 5b. Both the  $E_{gd}$  and  $E_{gi}$  values of these hybrid PNC films were found close to the  $E_g$  value of SnO<sub>2</sub> material and displayed a small, but linear decrease with increasing SnO<sub>2</sub> concentration. This result confirms that these PNCs could be used as band gap tuner in the designing of several next-generation important optoelectronic devices [18, 38, 39].

The interesting feature that can be noted from the insets of Fig. 5b is that the 1 wt% of SnO<sub>2</sub>-loaded PNC film has two different band gap values (the higher value is close to that of the PVP/PVA matrix and the lower one is nearly equal to that of the SnO<sub>2</sub> material) which can be tuned in a wide range by simply adjusting the nanofiller concentration around 1 wt%. The lowering of band gap for the 3 wt% and 5 wt% SnO<sub>2</sub> NPs-loaded PNC films can be explained by considering the charge transfer complexation (CTCs) which introduces different trap sites between the valence and conduction bands (localized states in the band gap) as explained for several other PNC materials [25, 39, 41, 47–49]. As a result of CTCs, both the lower and higher energies electronic transitions occurred when there was 1 wt% of SnO<sub>2</sub> loading in the PVP/PVA blend. However, the 3 wt% and 5 wt% of SnO<sub>2</sub> nanoinclusions in the PVP/PVA blend matrix had resulted in the dominance of the lower energy electronic transitions which led to a decrease of the energy band gap up to that of the SnO<sub>2</sub> material. This type of behavior could also be explained by considering the mechanism of localized surface plasmon resonance (LSPR) which was demonstrated earlier to understand the band gap behavior of CdCl<sub>2</sub>-doped PVP/PVA blend matrix-based composite films [26]. The LSPR phenomenon is collective oscillations of the electrons in a metallic nanostructure which occurs when there is sufficient transfer of electrons taking place from the functional groups of polymer macromolecules to that of the loaded nanofiller metal particles. This phenomenon is also sensitive to the size and shape of the nanostructures and that of the surrounding medium [50]. Further, it is an appreciably important phenomenon with regard to explore the suitability of such hybrid composite materials in optoelectronic, photonic, sensor, and organic light-emitting diode applications [18, 23, 25, 26, 31, 38, 41].



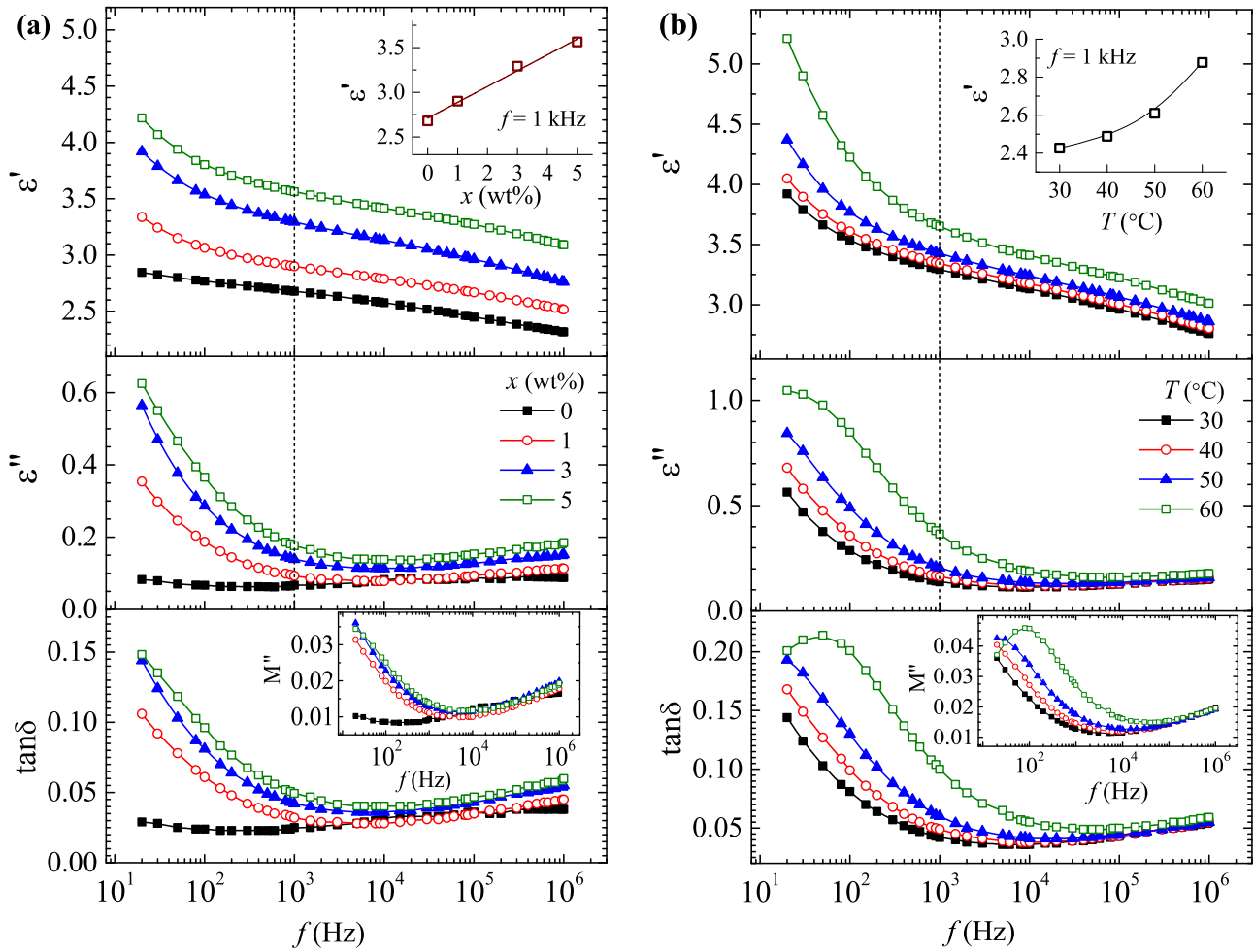


**Fig. 6** The plots of  $\epsilon'$ ,  $\epsilon''$ , and  $\tan\delta$  versus frequency  $f$  for **a** (PVP/PVA)/ $x$  wt% SnO<sub>2</sub> films at 30 °C and **b** (PVP/PVA)/3 wt% SnO<sub>2</sub> film with varying temperature. Insets given in the upper layers explain the variation of  $\epsilon'$  with  $x$  (wt%) of nanofiller for various

PNC films and the  $\epsilon'$  versus temperature  $T$  (°C) of the 3 wt% SnO<sub>2</sub>-loaded PNC film. The insets in lower layers display the loss part of electric modulus  $M''$  versus frequency  $f$  plots

### 3.6 Complex permittivity and analysis of dielectric polarization processes

Figure 6 shows the complex dielectric permittivity function (real part  $\epsilon'$  and imaginary part  $\epsilon''$ ) and the dielectric loss tangent ( $\tan\delta = \epsilon''/\epsilon'$ ) versus frequency  $f$  plots of the (PVP/PVA)/ $x$  wt% SnO<sub>2</sub> films of varying SnO<sub>2</sub> concentration at a steady temperature of 30 °C and also for the 3 wt% of SnO<sub>2</sub>-dispersed PNC film at different temperatures i.e., 30 °C, 40 °C, 50 °C, and 60 °C. These  $\epsilon'$  values of the PVP/PVA blend film at 30 °C decreased almost linearly from 2.85 to 2.32 with the increase of experimental frequency starting from 20 Hz and ending at 1 MHz. With the variation of six orders magnitude in frequency, the change in  $\epsilon'$  values of this PVP/PVA

blend film was found about 20% suggesting that this transparent film can serve as a flexible low permittivity dielectric over a broad frequency range. Further, the  $\epsilon'$  values of the fixed compositional ratio PVP/PVA blend film (50/50 wt%) were found in agreement with that published elsewhere [25]. Furthermore, the  $\epsilon''$  and  $\tan\delta$  values were also noted small for the PVP/PVA blend film and these dielectric functions were found almost frequency independent over the experimental range. The  $\epsilon'$  values of these (PVP/PVA)/SnO<sub>2</sub> hybrid materials were found reasonably higher than that of the host PVP/PVA blend matrix film and also increased with the increase of SnO<sub>2</sub> concentration. Additionally, the decrease in  $\epsilon'$  values of these PNCs was found non-linear in the frequency range of 20 Hz to 1 kHz,

whereas they had a linear decrease in the range starting around 1 kHz and ending at 1 MHz. These non-linear and linear dispersion regions of the  $\epsilon'$  values for the PNC films are separated by a vertical dashed line in the figure as a guide to the eye. This type of  $\epsilon'$  dispersion evidences that there was a significant involvement of the interfacial polarization (IP) in the  $\epsilon'$  values of lower experimental frequencies, but the higher experimental frequencies  $\epsilon'$  values attributed principally to the dipolar polarization of these polar polymers. The increase of SnO<sub>2</sub> amount enhanced the  $\epsilon'$  value of these PNCs which was expected because of the high  $\epsilon'$  values of the SnO<sub>2</sub> material ( $\epsilon' = 250$  at the electrical field of 1 kHz and 27 °C) [35] in contrast to that of the host PVP/PVA blend matrix (i.e.,  $\epsilon' = 2.7$  at 1 kHz and 30 °C determined in this work).

In contrast to the slow non-linear dispersion of  $\epsilon'$  in the range of 20 Hz to 1 kHz, the  $\epsilon''$  and  $\tan\delta$  decreased sharply which evidences a large contribution of the interfacial polarization process in this range. It is also expected from these spectra that the relaxation process peak may have evolved below 20 Hz at the film temperature of 30 °C. Furthermore, the  $\epsilon''$  and  $\tan\delta$  spectra have exhibited a broader minimum in the intermediate frequency span and then slowly increased with the further increase of frequency in the higher frequency span of the spectra. The inset given in the upper layer of Fig. 6a demonstrates the  $\epsilon'$  values for these PNC materials at a fixed frequency of 1 kHz which has enhanced linearly with the increasing SnO<sub>2</sub> concentration. This finding confirms the SnO<sub>2</sub> nanofiller concentration tunable dielectric permittivity of these (PVP/PVA)/SnO<sub>2</sub> hybrid composites confirming their effective uses as flexible PNDs in the microelectronic industries [3, 33, 43].

Figure 6b illustrates the dielectric polarization and dispersion behavior of the (PVP/PVA)/3 wt% SnO<sub>2</sub> composite as a representative sample at varying film temperatures. One can understand from this figure that there was an increase in  $\epsilon'$ ,  $\epsilon''$ , and  $\tan\delta$  values at a fixed frequency when the temperature of the PNC film augmented from 30 to 60 °C. This result attributes to the rise in thermally activated interfacial and dipolar polarization, and also the relaxation behavior which had been usually detected in several hybrid PNC materials [12, 18, 51]. The inset shown in the upper layer of Fig. 6b illustrates that there was a non-linear growth in the  $\epsilon'$  values (at a fixed

frequency e.g., 1 kHz) with the increased temperature of the film. Further, the PNC film at 60 °C exhibited a relaxation peak of Maxwell–Wagner–Sillars (MWS) dynamical mechanism that is around 50 Hz in the  $\tan\delta$  spectrum. The trend of these  $\tan\delta$  spectra also infer that the MWS dynamical process could have occurred at lower frequencies i.e., < 20 Hz for this PNC film when its temperature was kept below 60 °C.

The analysis of electrical modulus  $M''$  spectra of the hybrid composite materials provide better insight into the possible relaxations of their various dynamical processes [15, 16, 37–39, 51]. Therefore, the  $M''$  spectra for the (PVP/PVA)/SnO<sub>2</sub> hybrid PNC films were determined and are depicted at a fixed temperature as an inset in the lower layer of Fig. 6a. The  $M''$  spectra at different temperatures for the 3 wt% of SnO<sub>2</sub>-loaded PNC film are depicted in the lower layer inset of Fig. 6b. The advantage of using the  $M''$  function is that the various unwanted effects those contributed in the  $\epsilon''$  function are suppressed in the  $M''$  spectra [16, 45, 51]. The  $M''$  spectra of (PVP/PVA)/SnO<sub>2</sub> film has not displayed any dynamical process associated relaxation peak in this experimental frequency window. But it seemed that there could be relaxation peak lower than 20 Hz matching the IP dynamical process. The  $M''$  spectra at various temperatures for the 3 wt% of SnO<sub>2</sub>-loaded PNC film also exhibited relaxation peaks around 20 Hz and 100 Hz, respectively at the film temperatures of 50 °C and 60 °C. This relaxation process was only observed at 60 °C around 50 Hz in the  $\tan\delta$  spectrum and the same have not appeared at 50 °C for this film in the used experimental frequency range.

### 3.7 AC electrical conductivity behavior

The real part  $\sigma'$  of AC electrical conductivity for the (PVP/PVA)/SnO<sub>2</sub> films determined at 30 °C are plotted against frequency in Fig. 7a and also at different temperatures for the 3 wt% of SnO<sub>2</sub>-loaded PNC film in Fig. 7b. The  $\sigma'$  spectra of all these hybrid PNC materials displayed two distinct linear regions separated around 1 kHz i.e., first in the range 20 Hz to 1 kHz and then from about 1 kHz to 1 MHz which are definitely attributed to the semicrystalline nature of these hybrid composite materials as reported for several other semicrystalline PNCs [18, 41]. Further, it was noted that the low-frequency linear region had a relatively lower value of the slope as compared to

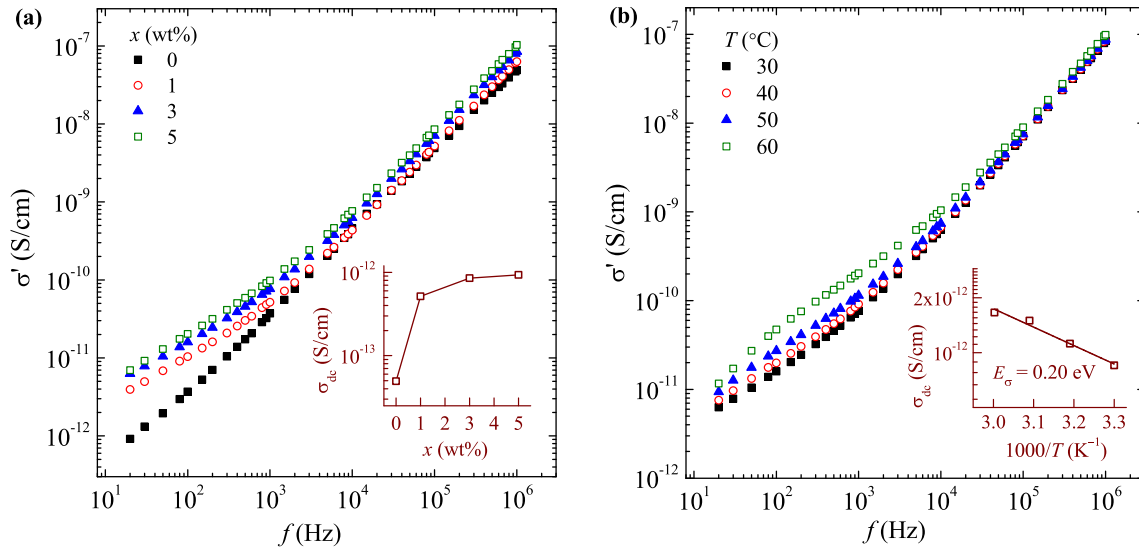


**Fig. 7** The  $\sigma'$  plots as a function of frequency  $f$  for **a** (PVP/PVA)/ $x$  wt% SnO<sub>2</sub> films at 30 °C and **b** (PVP/PVA)/3 wt% SnO<sub>2</sub> film with varying temperature. Insets depict the plots of  $\sigma_{dc}$  against

$x$  (wt%) concentration of nanofiller for these PNC materials and Arrhenius behavior ( $\sigma_{dc}$  versus  $1000/T$ ) for the 3 wt% SnO<sub>2</sub>-loaded PNC film

that of the high-frequency linear dispersion of the  $\sigma'$  spectra for all these composite materials. Furthermore, the direct current (DC) electrical conductivity ( $\sigma_{dc}$ ) values (which were computed from the linear portion of the lower frequency region by extrapolating it to zero frequency intercept on the  $\sigma'$  axis) were found high for the PNC films in comparison to their host PVP/PVA matrix. From the inset of Fig. 7a, it can be learned that the  $\sigma_{dc}$  values increased largely with the 1 wt% of SnO<sub>2</sub> dispersion and then increased relatively less with the further increase of SnO<sub>2</sub> concentration up to 5 wt% in the (PVP/PVA)/SnO<sub>2</sub> films. These outcomes also evidence that the loading of SnO<sub>2</sub> nanoparticles in the PVP/PVA blend has developed some favorable charge conducting paths which promoted the charge mobility and thereby increased the electrical conductivity of these hybrid composite materials.

Figure 7b explains that the  $\sigma'$  values of (PVP/PVA)/3 wt% SnO<sub>2</sub> film were sufficiently enhanced below 10 kHz when the film temperature was increased from 30 to 60 °C, while the increase in  $\sigma'$  values was found relatively insignificant above 100 kHz. The Arrhenius plot of the  $\sigma_{dc}$  values versus  $1000/T$  is shown in the inset of Fig. 7b from which the activation energy of electrical conduction  $E_{\sigma}$  was found to be 0.20 eV for this 3 wt% of SnO<sub>2</sub>-loaded PNC film. The small  $E_{\sigma}$  value is interesting for use of these materials as host matrices for the preparation of promising ionic conductivity-bearing solid-state

electrolytes with the addition of some alkali metal salts similar to that demonstrated in the literature [52].

### 4 Conclusion

The detailed structural properties, temperatures of the thermodynamical processes, UV absorbance energy band gaps, and the dielectric permittivity and ac electrical conductivity behavior of the (PVP/PVA)/SnO<sub>2</sub> nanocomposites were reported. These results are of great interest from the current polymer technology-based advances in flexible electronics. It was found that the dispersion of small amounts of SnO<sub>2</sub> nanoparticles (i.e., 1 wt%, 3 wt%, and 5 wt%) in the host PVP/PVA blend matrix of 50/50 wt% compositional ratio evolved promising thermal, optical, and dielectric properties of the resultant PNC films. The morphology of PVP/PVA blend film was noted as highly smooth which turned slightly uneven when the SnO<sub>2</sub> NPs were loaded in the blend matrix. The percent degree of crystallinity and thermal stability of these hybrid nanocomposites progressively increased with increasing SnO<sub>2</sub> amounts. The UV–Vis absorbance was significantly enhanced and the energy band gap decreased with the rise of SnO<sub>2</sub> nanofiller concentration in these PNC films. Optical properties confirm the suitability of these nanocomposites as UV shielders, UV detectors, and the energy band gap

tuner materials for developing numerous next-generation biodegradable optoelectronic devices. The increased dielectric permittivity and the electrical conductivity with the loading of SnO<sub>2</sub> NPs in the PVP/PVA blend confirm these flexible nanocomposites as potential candidates of tunable-type nanodielectrics. Such dielectric could be used as a substrate and insulator for developing a variety of high-performance biodegradable microelectronic devices for advances in next-generation flexible and stretchable-type device technologies.

## Acknowledgements

The University Grants Commission of India, New Delhi is gratefully acknowledged for SAP DRS-II Grant No. F.530/12/DRS-II/2016(SAP-I) for establishing some experimental facilities for RJS. One of the authors (PD) thanks the CSIR, New Delhi for honoring her work by a postdoctoral research associate fellowship.

## Declarations

**Conflict of interest** The authors declare that they have no conflict of interest.

## References

1. M. Teodorescu, M. Bercea, Poly(vinylpyrrolidone)—a versatile polymer for biomedical and beyond medical applications. *Polym. Plast. Tech. Eng.* **54**, 923–943 (2015)
2. N.B. Halima, Poly(vinyl alcohol): review of its promising applications and insights into biodegradation. *RSC Adv.* **6**, 39823–39832 (2016)
3. P. Dhatarwal, S. Choudhary, R.J. Sengwa, Effectively nanofiller concentration tunable dielectric properties of PVP/SnO<sub>2</sub> nanodielectrics. *Mater. Lett.* **273**, 127913 (2020)
4. R.J. Sengwa, S. Choudhary, Investigation of correlation between dielectric parameters and nanostructures in aqueous solution grown poly(vinyl alcohol)-montmorillonite clay nanocomposites by dielectric relaxation spectroscopy. *Express Polym. Lett.* **4**, 559–569 (2010)
5. M. Kumar, P. Devi, A. Kumar, Structural analysis of PVP capped silver nanoparticles synthesized at room temperature for optical, electrical and gas sensing properties. *J. Mater. Sci.: Mater. Electron.* **28**, 5014–5020 (2017)
6. A.O. Turkey, A. Barhoum, M.M. Rashad, M. Bechlany, Enhanced the structure and optical properties for ZnO/PVP nanofibers fabricated via electrospinning technique. *J. Mater. Sci.: Mater. Electron.* **28**, 17526–17532 (2017)
7. P. Dhatarwal, R.J. Sengwa, Enhanced dielectric properties of the ZnO and TiO<sub>2</sub> nanoparticles dispersed poly(vinyl pyrrolidone) matrix-based nanocomposites. *J. Macromol. Sci. B* **59**, 853–866 (2020)
8. D. Wang, S.-C. Chen, Q. Zheng, Poly(vinylpyrrolidone)-doped SnO<sub>2</sub> as an electron transport layer for perovskite solar cells with improved performance. *J. Mater. Chem. C* **7**, 12204–12210 (2019)
9. K.K. Sadasivuni, J.J. Cabibihan, D. Ponnamma, M.A. AlMaadeed, J. Kim, *Bipolymer Composites in Electronics* (Elsevier Inc., Amsterdam, 2017).
10. R. Ambrosio, A. Carrillo, M.L. Mota, K. de la Torre, R. Torrealba, M. Moreno, H. Vazquez, J. Flores, I. Vivaldo, Polymeric nanocomposites membranes with high permittivity based on PVA-ZnO nanoparticles for potential applications in flexible electronics. *Polymers* **10**, 1370 (2018)
11. F. Xu, H. Zhang, L. Jin, Y. Li, J. Li, G. Gan, M. Wei, M. Li, Y. Liao, Controllably degradable transient electronic antennas based on water-soluble PVA/TiO<sub>2</sub> films. *J. Mater. Sci.* **53**, 2638–2647 (2018)
12. I.S. Yahia, M.I. Mohammed, Facile synthesis of graphene oxide/PVA nanocomposites for laser optical limiting: band gap analysis and dielectric constants. *J. Mater. Sci.: Mater. Electron.* **29**, 8555–8563 (2018)
13. R.J. Sengwa, S. Sankhla, Dielectric dispersion study of coexisting phases of aqueous polymeric solution: poly (vinyl alcohol)+poly (vinyl pyrrolidone) two-phase systems. *Polymer* **48**, 2737–2744 (2007)
14. Q. Wei, Y. Zhang, Y. Wang, W. Chai, M. Yang, Measurement and modeling of the effect of composition ratios on the properties of poly(vinyl alcohol)/poly(vinyl pyrrolidone) membranes. *Mater. Des.* **103**, 249–258 (2016)
15. A.Y. Yassin, Dielectric spectroscopy characterization of relaxation in composite based on (PVA–PVP) blend for nickel–cadmium batteries. *J. Mater. Sci.: Mater. Electron.* **31**, 19447–19463 (2020)
16. E.M. Abdelrazek, A.M. Abdelghany, A.E. Tarabiah, H.M. Zidan, AC conductivity and dielectric characteristics of PVA/PVP nanocomposite filled with MWCNTs. *J. Mater. Sci.: Mater. Electron.* **30**, 15521–15533 (2019)
17. M.T. Ramesan, P. Jayakrishnan, T. Anilkumar, G. Mathew, Influence of copper sulphide nanoparticles on the structural, mechanical and dielectric properties of poly(vinyl alcohol)/poly(vinyl pyrrolidone) blend nanocomposites. *J. Mater. Sci.: Mater. Electron.* **29**, 1992–2000 (2018)
18. S. Choudhary, R.J. Sengwa, ZnO nanoparticles dispersed PVA–PVP blend matrix based high performance flexible

- nanodielectrics for multifunctional microelectronic devices. *Curr. Appl. Phys.* **18**, 1041–1058 (2018)
19. R.J. Sengwa, S. Sankhla, S. Choudhary, Dielectric characterization of solution intercalation and melt intercalation poly(vinyl alcohol)–poly(vinyl pyrrolidone) blend–montmorillonite clay nanocomposite films. *Indian J. Pure Appl. Phys.* **48**, 196–204 (2010)
  20. B.M. Baraker, B. Lobo, UV irradiation induced microstructural changes in CdCl<sub>2</sub> doped PVA–PVP blend. *J. Mater. Sci.: Mater. Electron.* **29**, 4106–4121 (2018)
  21. B. Guruswamy, V. Ravindrachary, C. Shruthi, S. Hegde, R.N. Sagar, S.D. Praveen, Optical, electrical and thermal properties of SnO<sub>2</sub> nanoparticles doped poly vinyl alcohol–poly vinyl pyrrolidone blend polymer electrolyte. *Indian J. Adv. Chem. Sci.* **6**, 17–20 (2018)
  22. W.N.A. Aziz, A. Bumajdad, F. Al Sagheer, M. Madkour, Selective synthesis and characterization of iron oxide nanoparticles via PVA/PVP polymer blend as structure-directing agent. *Mater. Chem. Phys.* **249**, 122927 (2020)
  23. F.M. Ali, R.M. Kersh, Synthesis and characterization of La<sup>3+</sup> ions incorporated (PVA/PVP) polymer composite films for optoelectronics devices. *J. Mater. Sci.: Mater. Electron.* **31**, 2557–2566 (2020)
  24. B. Guruswamy, V. Ravindrachary, C. Shruthi, M. Mylarappa, Effect of SnO<sub>2</sub> nanoparticle doping on structural, morphological and thermal properties of PVA–PVP polymer blend. *Mater. Sci. Forum* **962**, 82–88 (2019)
  25. K. Rajesh, V. Crasta, N.B.R. Kumar, G. Shetty, Y. Sangappa, J. Kudva, Effect of MoO<sub>3</sub> nanofiller on structural, optical, mechanical, dielectric and thermal properties of PVA/PVP blend. *Mater. Res. Innov.* **24**, 270–278 (2020)
  26. B.M. Baraker, B. Lobo, Spectroscopic analysis of CdCl<sub>2</sub> doped PVA–PVP blend films. *Can. J. Phys.* **95**, 738–747 (2017)
  27. S. Choudhary, P. Dhatarwal, R.J. Sengwa, Influence of SnO<sub>2</sub> nano-inclusions on the structural and dielectric properties of (PVA–PEO)/SnO<sub>2</sub> nanocomposites. *Indian J. Chem. Technol.* **27**, 367–374 (2020)
  28. S. Senthil, S. Srinivasan, T. Thangeeswari, V. Ratchagar, Enrichment of optical, magnetic and photocatalytic properties in PVP capped CdO/SnO<sub>2</sub> nanocomposites synthesized by microwave irradiation method. *J. Mater. Sci.: Mater. Electron.* **30**, 19841–19853 (2019)
  29. V.S. Reddy Channu, B. Rambabu, K. Kumari, R.R. Kalluru, R. Holze, SnO<sub>2</sub>/PANI nanocomposite electrodes for supercapacitors and lithium ion batteries. *Electrochim. Energy Technol.* **4**, 32–38 (2018)
  30. A. Husain, S. Ahmad, F. Mohammad, Electrical conductivity and alcohol sensing studies on polythiophene/tin oxide–nanocomposites. *J. Sci.: Adv. Mater. Dev.* **5**, 84–94 (2020)
  31. P.K. Sarkar, S. Bhattacharjee, M. Prajapat, S. Roy, Incorporation of SnO<sub>2</sub> nanoparticles in PMMA for performance enhancement of a transparent organic resistive memory device. *RSC Adv.* **5**, 105661–105667 (2015)
  32. P. Dhatarwal, S. Choudhary, R.J. Sengwa, Significantly enhanced dielectric properties and chain segmental dynamics of PEO/SnO<sub>2</sub> nanocomposites. *Polym. Bull.* (2020). <https://doi.org/10.1007/s00289-020-03215-2>
  33. P. Dhatarwal, R.J. Sengwa, S. Choudhary, Multifunctional (PVP/PEO)/SnO<sub>2</sub> nanocomposites of tunable optical and dielectric properties. *Optik* **221**, 165368 (2020)
  34. K.G. Dhinakar, T. Selvalakshmi, S.M. Sundar, A.C. Bose, Structural, optical and impedance properties of SnO<sub>2</sub> nanoparticles. *J. Mater. Sci.: Mater. Electron.* **27**, 5818–5824 (2016)
  35. A. Azam, A.S. Ahmed, M. Chaman, A.H. Naqvi, Investigation of electrical properties of Mn doped tin oxide nanoparticle using impedance spectroscopy. *J. Appl. Phys.* **108**, 094329 (2010)
  36. M.O. Orlandi, *Tin Oxide Materials: Synthesis, Properties, and Applications* (Elsevier Inc., Amsterdam, 2020).
  37. P. Dhatarwal, R.J. Sengwa, Tunable β-phase crystals, degree of crystallinity, and dielectric properties of three-phase PVDF/PEO/SiO<sub>2</sub> hybrid polymer nanocomposites. *Mater. Res. Bull.* **129**, 110901 (2020)
  38. R.J. Sengwa, S. Choudhary, P. Dhatarwal, Nonlinear optical and dielectric properties of TiO<sub>2</sub> nanoparticles incorporated PEO/PVP blend matrix based multifunctional polymer nanocomposites. *J. Mater. Sci.: Mater. Electron.* **30**, 12275–12294 (2019)
  39. P. Dhatarwal, R.J. Sengwa, Structural, dielectric dispersion and relaxation, and optical properties of multiphase semicrystalline PEO/PMMA/ZnO nanocomposites. *Compos. Interfaces* (2020). <https://doi.org/10.1080/09276440.2020.1813474>
  40. P. Dhatarwal, R.J. Sengwa, Impact of PVDF/PEO blend composition on the β-phase crystallization and dielectric properties of silica nanoparticles incorporated polymer nanocomposites. *J. Polym. Res.* **26**, 196 (2019)
  41. R.J. Sengwa, P. Dhatarwal, S. Choudhary, A comparative study of different metal oxide nanoparticles dispersed PVDF/PEO blend matrix-based advanced multifunctional nanodielectrics for flexible electronic devices. *Mater. Today Commun.* **25**, 101380 (2020)
  42. R.J. Sengwa, S. Choudhary, Structural characterization of hydrophilic polymer blends/montmorillonite clay nanocomposites. *J. Appl. Polym. Sci.* **131**, 40617 (2014)
  43. D.Q. Tan, Review of polymer-based nanodielectric exploration and film scale-up for advanced capacitors. *Adv. Funct. Mater.* **30**, 1808567 (2020)

44. H. Luo, X. Zhou, C. Ellingford, Y. Zhang, S. Chen, K. Zhou, D. Zhang, C.R. Bowen, C. Wan, Interface design for high energy density polymer nanocomposites. *Chem. Soc. Rev.* **48**, 4424–4465 (2019)
45. M.A. Morsi, A. Rajeh, A.A. Al-Muntaser, Reinforcement of the optical, thermal and electrical properties of PEO based on MWCNTs/Au hybrid fillers: nanodielectric materials for organoelectronic devices. *Compos. B* **173**, 106957 (2019)
46. J. Tauc, A. Menth, D.L. Wood, Optical and magnetic investigations of the localized states in semiconducting glasses. *Phys. Rev. Lett.* **25**, 749–752 (1970)
47. S.B. Aziz, M.A. Rasheed, H.M. Ahmed, Synthesis of polymer nanocomposites based on [methyl cellulose]<sub>(1-x)</sub>:(CuS)<sub>x</sub> (0.02 M ≤ x ≤ 0.08 M) with desired optical band gaps. *Polymers* **9**, 194 (2017)
48. M.S.A. Hussien, M.I. Mohammed, I.S. Yahia, Flexible photocatalytic membrane based on CdS/PMMA polymeric nanocomposite films: multifunctional materials. *Environ. Sci. Pollut. Res.* **27**, 45225–45237 (2020)
49. R.J. Sengwa, P. Dhatarwal, Polymer nanocomposites comprising PMMA matrix and ZnO, SnO<sub>2</sub>, and TiO<sub>2</sub> nanofillers: a comparative study of structural, optical, and dielectric properties for multifunctional technological applications. *Opt. Mater.* **113**, 110837 (2021)
50. J. Zheng, C. Zhang, R.M. Dickson, Highly fluorescent, water-soluble, size-tunable gold quantum dots. *Phys. Rev. Lett.* **93**, 077402 (2004)
51. P. Dhatarwal, R.J. Sengwa, Structural and dielectric characterization of (PVP/PEO)/Al<sub>2</sub>O<sub>3</sub> nanocomposites for biodegradable nanodielectric applications. *Adv. Compos. Hybrid Mater.* **3**, 344–353 (2020)
52. R.J. Sengwa, P. Dhatarwal, Predominantly chain segmental relaxation dependent ionic conductivity of multiphase semicrystalline PVDF/PEO/LiClO<sub>4</sub> solid polymer electrolytes. *Electrochim. Acta* **338**, 135890 (2020)

**Publisher's Note** Springer Nature remains neutral with regard to jurisdictional claims in published maps and institutional affiliations.